JOURNAL OF PROPULSION AND POWER
Vol. 25, No. 5, September–October 2009

Characterization of Nanothermite Material for Solid-Fuel Microthruster Applications

Steven J. Apperson,* Andrey V. Bezmelnitsyn,† Rajagopalan Thiruvengadathan,†
Keshab Gangopadhyay,‡ and Shubhra Gangopadhyay§
University of Missouri, Columbia, Missouri 65211
and
Wendy A. Balas,¶ Paul E. Anderson,** and Steven M. Nicolich††
U.S. Army, Picatinny, New Jersey 07896

DOI: 10.2514/1.43206

Nanothermite composites containing metallic fuel and inorganic oxidizer have unique combustion properties that make them potentially useful for microthruster applications. The thrust-generating characteristics of copper oxide/aluminum nanothermites have been investigated. The mixture was tested in various quantities (9–38 mg) by pressing the material over a range of densities. The testing was done in two different types of thrust motors: one with no nozzle and one with a convergent–divergent nozzle. As the packing density was varied, it was found that the material exhibited two distinct impulse characteristics. At low packing pressure, the combustion was in the fast regime, and the resulting thrust forces were ∼75 N with a duration of less than 50 μs full width at half-maximum. At high density, the combustion was relatively slow and the thrust forces were 3–5 N with a duration 1.5–3 ms. In both regimes, the specific impulse generated by the material was 20–25 s. The specific impulse and short thrust duration created by this unique nanothermite material makes it promising for micropropulsion applications, in which space is limited.

I. Introduction

RECENT research has demonstrated that microthrusters can be designed to reliably create thrust impulses in the impulse ranges defined as microthrusters (∼10 μN to 10 N ranges) [1–7]. The fuels used in such systems include lead styphnate, glycidyl azide polymer composites, composites of double base (DB) and black powder (BP), BTATz, and DAATO3.5 [1–6]. A microthruster containing ∼7 mg of DB + 30%BP produced a measured thrust of 1 mN, a duration of 1.15 s, and total impulse of 1.13 mN · s [3]. Another recent work reported on a quartz thruster containing DAATO3.5 capable of producing 100 mN of peak thrust over a duration of ∼80 ms and a total impulse of ∼20 mN · s [1]. These propellants have combustion rates ranging from 5–100 mm/s. Another set of work has demonstrated thrusters using gunpowder-based propellants that produced up to 0.38 N of peak thrust in a duration of ∼0.4 ms [5].

Certain applications of solid-propellant microthrusters, such as course correction of high-velocity projectiles or microsatellites, require that the actuation time be as short as possible. For example, lateral guidance of spin-stabilized projectiles requires short-duration thrust to avoid rotation of the thrust vector as the projectile spins. Considering a projectile rotating at greater than 200 Hz, a thrust duration of 0.4 ms would correspond to a projectile rotation of ∼29 deg. For such applications, the fuel should be chosen to have the highest possible combustion rate, thereby minimizing movement of the thrust vector. However, the thrust fuel should not detonate, which would lead to damage of the projectile.

It was recently shown that the nanothermite composite consisting of CuO nanorods mixed with Al nanoparticles is capable of producing reaction propagation rates similar to those of conventional primary explosives, but with pressure levels well below that of solid explosives [8]. This characteristic makes the composite a promising candidate for fast-impulse microthruster applications. It was found that this nanothermite composite is capable of producing shock waves with Mach numbers up to 2.44 in an air-filled tube [8].

In this paper, the thrust performance of a nanothermite composite (CuO nanorods and Al nanoparticles) in a simple prototype thruster motor is presented. This composite was tested at a wide range of packing densities in a motor without any nozzle, as well as in a motor with a convergent–divergent nozzle.

Received 13 January 2009; revision received 21 April 2009; accepted for publication 23 April 2009.

*Graduate Research Assistant, Department of Electrical & Computer Engineering, Room 349, Engineering Building West; sja895@mizzou.edu.
†Research Assistant Professor, Department of Electrical & Computer Engineering, Room 349, Engineering Building West.
‡Research Professor, Department of Nuclear Engineering, Room 349, Engineering Building West.
§Professor, Department of Electrical and Computer Engineering, Room 349, Engineering Building West; gangopadhyays@missouri.edu.
¶Chemical Engineer, Armament Research Development and Engineering Center, Energetics and Warheads Division, Building 3028.
**Chemist, Armament Research Development and Engineering Center, Energetics and Warheads Division, Building 3028.
††Division Chief, Armament Research Development and Engineering Center, Energetics and Warheads Division, Building 3022.

II. Experimental

A. Nanothermite Preparation

The nanothermite composition consisted of CuO nanorods and Al nanoparticles. The CuO nanorods were synthesized using the surfactant templating process, described elsewhere [9]. The aluminum nanoparticles were purchased from Novacentrix, with an average diameter of 80 nm and an average Al_2O_3 shell thickness of 2.2 nm. First, a slurry was prepared by dispersing CuO nanorods in 2-propanol by sonication for 30 min. Then the aluminum nanoparticles were added to the slurry, and it was sonicated for 4 h. The sonication was carried out using a Cole-Parmer ultrasonic cleaning bath. After mixing, the slurry was dried in an oven at 90°C until all the 2-propanol was removed. The mixing ratio of the composite was 17:40 (Al:CuO) by weight. This ratio had been previously optimized for maximum combustion rate [9]. The optimized equivalence ratio will lead to the maximum conversion of the reactants into products.

B. Thruster Prototype Design

The thrust motors designed for testing the nanothermite was fabricated by boring out stainless steel bolts. The inner diameter of the chamber was 1/16 in. (1.59 mm). Three motors were fabricated with different chamber lengths (3.5, 6, and 8.5 mm). In addition, one motor was fabricated with a convergent–divergent nozzle. A schematic of the motor designs is shown in Fig. 1.

The fabrication was carried out using a precision lathe. The diameter of the chambers was defined by the diameter of the drill bit used for boring out the chambers. The thruster with no nozzle was fabricated by drilling in a set depth from one side and then bottoming out the base of the chamber. The thruster with the convergent–divergent nozzle was fabricated by boring in from both sides. The chamber was bored out from one direction (from the left, as oriented in Fig. 1b) using a drill bit with a 118 deg tip angle. Then the divergence of the nozzle was created by drilling in from the other direction (from the right, as oriented in Fig. 1b) using a drill bit with a 30 deg tip angle. The depth of drilling from each side was controlled using the calibrated hand wheels on the carriage. This fabrication method resulted in the chamber being open at the base. This was sealed shut using a threaded plug coated with epoxy.

The motors were loaded using a hydraulic press. This allowed precise loading with a desired packing pressure. The material was loaded incrementally in 2–3 mg iterations (estimated from total loaded mass and number of loading iterations) and pressed each time. This ensured uniform pressing and therefore uniform density of the fully loaded composite. The material was loaded until the chamber was completely filled; therefore, at higher pressure, more material was loaded into the chamber. Seven different packing pressures were tested from 1.26 MPa (∼183 psi) up to 630 MPa (∼91,000 psi) using the motor with a 3.5-mm-long chamber and no nozzle. The resulting percentage of theoretical maximum density (%TMD) for this range of pressures was 28.0 to 64.9%. The %TMD is based on a calculated TMD of 5.36 g/cm^3 for the present CuO/Al nanothermite mixture.

In addition to comparing the effect of different packing densities, the three different lengths of chamber were tested, and the motor with a convergent–divergent nozzle (Fig. 1b) was compared with the motor with no nozzle. The motor with no nozzle was loaded through the top, and the motor with the convergent–divergent nozzle was loaded through the bottom and then sealed using a plug as described previously. All of the different motors with and without the convergent–divergent nozzle were tested at both high packing pressure (315 MPa) and low packing pressure (6.3 MPa). All the motors were reusable, because they were able to be reloaded after each use. The motors were weighted between each test to verify that there was no loss in mass (erosion of the thrust chamber or nozzle). Every experimental condition was tested 4 times to obtain an average. A list of experiments performed and the variables is shown in Table 1.

C. Thruster Test Stand

A schematic of the test stand is shown in Fig. 2. The thrust motor was mounted vertically on a force sensor (Kistler type 9222). The ignition was triggered using a fuse wire coated with the nanothermite composite. The fuse wire was not in physical contact with the thrust motor, but it was within 2 mm to allow the reaction to jump from the fuse wire to the material in the motor. The exhaust plume was recorded with a high-speed camera (Photron Fastcam SA-1.1). The resolution was 192 × 512, the frame rate was 40,000 frames/second, and the shutter speed was 370 ns. The fuse-wire ignition, force-sensor data acquisition (DAQ), and camera recording were triggered synchronously using a dc battery and a push-button switch. The sensor (Kistler type 9222) was plugged into a charge amplifier (Kistler type 5010B), and the amplifier output signal was sent to a National Instruments DAQ board (PCI-6110).

III. Results and Discussion

A. Effect of Packing Density

The percentage of theoretical maximum density versus packing pressure is shown in Fig. 3a. An approximately linear relationship between the logarithm of packing pressure and %TMD is expected for cold-pressing of powders [10]. Because the volume of the chamber was constant in this series of tests, the mass of the nanothermite varied directly with the packing density. The total impulse and mass versus packing pressure are shown in Fig. 3b. The total impulse varied similarly to the mass, which indicates that the thrust efficiency was almost constant.

The thrust efficiency is measured by the specific impulse I_{SP}, defined by Eq. (1):

$$I_{SP} = \left(\int F \cdot \mathrm{d}t\right) \Big/ W_P \tag{1}$$

where F is the measured thrust force, and W_P is the propellant weight. There did not appear to be any discernible correlation between the specific impulse and %TMD (Fig. 4a). More interestingly, however, when the pressing density was varied, two distinct reaction regimes were observed. Figure 4b is a plot of the peak thrust and impulse duration vs packing pressure. It can be seen from Fig. 4b that the peak thrust and impulse duration change by more than 1 order of magnitude when the reaction crosses from one regime to the other. At low densities (less than 44.4%TMD), the material had very fast combustion speed, and the resulting thrust was less than ∼50 μs in duration [full width at half-maximum (FWHM)] with a peak thrust greater than 40 N. At high pressure (greater than 44.4%TMD), the material had a very slow combustion rate, and the resulting thrust force was much lower (4–5 N).

As the packing density was varied from 28.0 to 64.9%TMD, the transition between regimes was not gradual. At 44.4%TMD, the reaction-regime transition was observed. The event began slowly, and then almost instantaneously, all the remaining material reacted, producing a very large spike in thrust force. Figure 4c shows example thrust pulses for each regime. This inverse relationship between packing density and reaction propagation rate has been observed for various nanothermites in other systems [8,10–12]. In particular, an abrupt combustion-rate transition of more than an order of magnitude has been observed when comparing pressed pellets of WO_3/Al pellets with loose powder [12].

The slow- and fast-reaction behaviors are also evident in the high-speed video recorded during the experiments. In the slow regime, the high-speed video shows that the material is ejected uniformly from the chamber. Figure 5a shows a sequence of frames from one test performed with material pressed to a %TMD of ∼56.0%, and Fig. 5b shows the thrust profile for the same test. The exhaust plume in Fig. 5a is a homogenous plume during the duration of the thrust

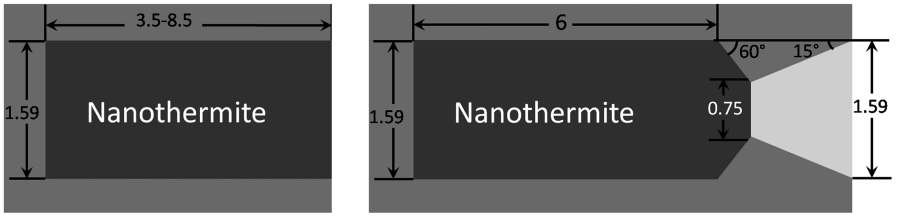

Fig. 1 Motor design a) without nozzle and b) with convergent–divergent nozzle. All dimensions are in millimeters.

Table 1 List of experimental conditions and variables tested

Packing Pressure, MPa	Chamber length, mm	Nozzle design
Variable (1.26–630)	3.5	No nozzle
6.30	Variable (3.5, 6.0, 8.5)	No nozzle
315.00	Variable (3.5, 6.0, 8.5)	No nozzle
6.30	6.0	Convergent–divergent
315.00	6.0	Convergent–divergent

shown in Fig. 5b. This thrust profile resembles a neutral burn, which is characteristic of an end-burning propellant grain, in which burn rate, temperature, and pressure remain almost constant during combustion [13].

On the other hand, in the fast regime, all the reaction products appear to be ejected almost simultaneously. Figure 6a shows a sequence of frames for a test with material pressed to 35.4%TMD. Figure 6b shows the force data corresponding to the video in Fig. 6a. It appears that most of the material has burned and been ejected by the fifth frame (74.7 ms). We believe that the rapid ejection of material may be caused by supersonic combustion behavior. If the combustion front propagates at supersonic velocity, then it would reach the bottom of the chamber before the material could be ejected. Then it would reflect off the bottom of the chamber and rapidly eject the rest of the material as a single mass. The ejected material most likely does not travel at supersonic rates at the thruster exit plane, but the combustion front leads to the collective ejection of the reaction products. These products are most likely in mixed phases of some solid, liquid, and vapor. The ejection of material by reflected wave fronts has been seen in combustion tubes when the ignition end is open and the opposite end is closed [14].

A possible explanation of two distinct reaction behaviors is that reaction propagation is dominated by conductive energy transfer in the slow-reaction regime, and the reaction propagation is dominated by convective energy transfer in the fast regime [12]. The density at which the transition occurs is related to the energetic material properties such as particle size and type of fuel and oxidizer. Additionally, in a small-scale system such as the present thruster, there will likely be external effects that influence this transition density. For example, the diameter and wall material of the chamber will affect energy losses and hence probably affect the density at which combustion-regime transition occurs.

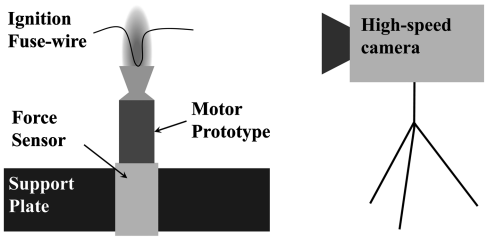

Fig. 2 Schematic of the thruster test stand.

B. Effect of Motor Length

After discovering that there were two distinct regimes of behavior, the effect of motor length was tested in each regime. The low-density regime was tested at 34.3%TMD and the high-density regime was tested at 56.0%TMD. Figure 7a shows the profile for each motor in the low-density regime, and Fig. 7b shows the profiles for the high-density regime. Each profile in Figs. 7a and 7b is a point-by-point average of profiles from four independent tests. The comparison in Fig. 7 shows the expected relationship when the length of the motor is increased. The duration of the thrust increases almost linearly, indicating a nearly constant reaction rate. The initial spike in the thrust profiles in Fig. 7b is from the reaction of the nanothermite coating on the fuse wire.

C. Nozzle Design Effect

The convergent–divergent nozzle design shown in Fig. 1b was tested for comparison with the thruster without a nozzle. This was tested in both the fast regime (at 34.3%TMD) and the slow regime (at 56.0%TMD). The thrust profile for the convergent–divergent nozzle compared with no nozzle in the fast regime is shown in Fig. 8a. The nozzle comparison for the slow regime is shown in Fig. 8b.

It is apparent from the data in Fig. 8a that the convergent–divergent nozzle reduces the amplitude (from ∼65 to ∼54 N) and increases the duration (from 55.0 to 83.4 μs FWHM) of the thrust profile in the fast regime. The specific impulse changes from 24.81 ± 0.41 s to 26.68 ± 0.82 s. In the slow regime, the nozzle increases the thrust (from ∼4.2 to ∼8 N) and reduces the duration (∼1.22 to ∼0.55 ms FWHM), as shown in Fig. 6b. The specific impulse changes from 28.27 ± 0.95 s to 24.82 ± 0.79 s.

In the slow-reaction regime, the convergent–divergent nozzle design increases the thrust force and reduces the thrust duration, as predicted by the rocket nozzle design theory [13]. The thrust force increases because the exhaust flow is accelerated through the diverging portion of the nozzle, increasing the exhaust velocity at the nozzle exit plane. In contrast, in the fast-reaction regime, the nozzle reduces the thrust force slightly and increases the duration (full width). However, from the plot in Fig. 8a, with the convergent–divergent nozzle, the thrust duration (FWHM) is narrower than without a nozzle. Then there is a tail-off of the thrust pulse that makes the total duration longer than without a nozzle.

Figures 9 and 10 show high-speed images of the fast-reaction regime with and without a convergent–divergent nozzle, respectively. Each of the images in Figs. 9 and 10 are separated by 100 μs. Both sequences show a rapid ejection of hot material, followed

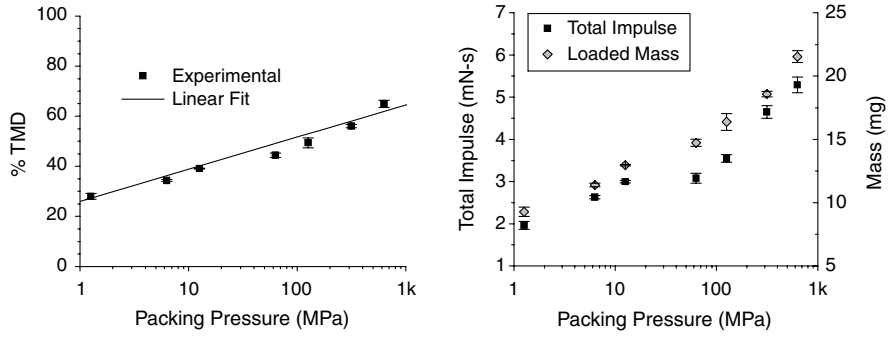

a) b)

Fig. 3 Plots of a) nanothermite density vs packing pressure and b) nanothermite mass and total impulse vs packing pressure.

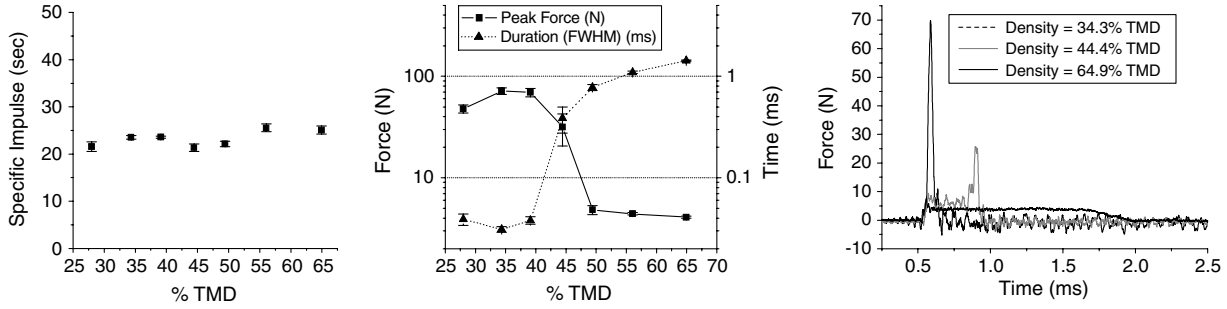

a) b) c)

Fig. 4 Plots of a) specific impulse vs %TMD, b) peak thrust and impulse duration vs packing pressure, and c) impulse profiles for three different packing pressures.

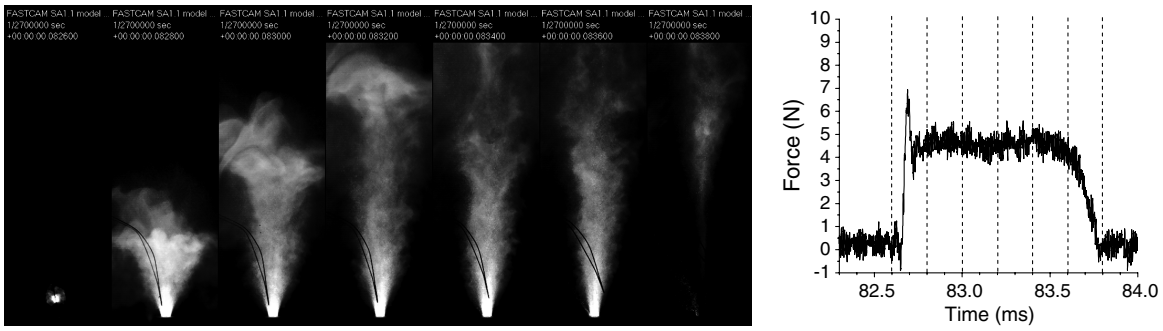

a) b)

Fig. 5 Exhaust plume from material pressed to 57.8%TMD: a) video frames and b) force data (dotted lines in the plot mark time stamps for the video frames).

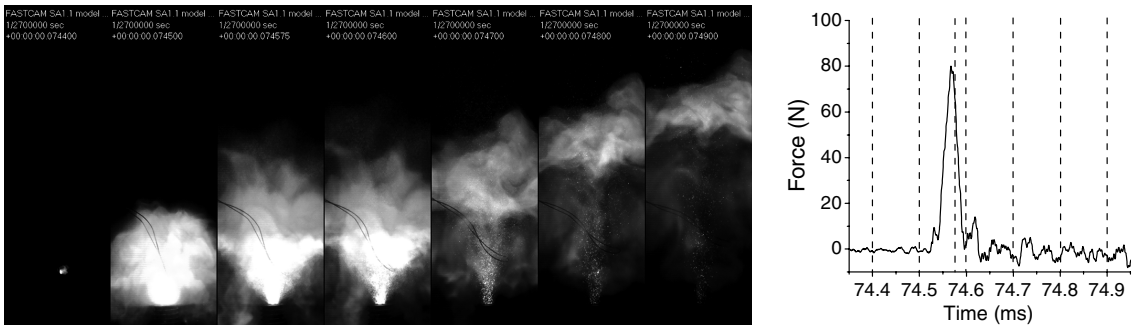

a) b)

Fig. 6 Exhaust plume from material pressed to 35.4%TMD: a) frame shots and b) force data (dotted lines in the plot mark time stamps for the video frames).

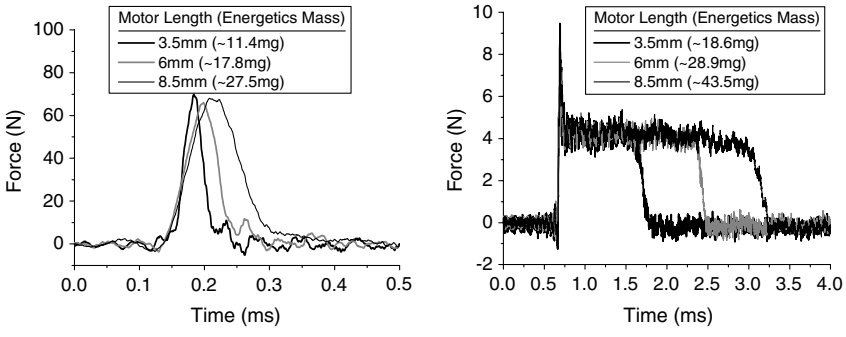

a) b)

Fig. 7 Thrust profiles for different motor lengths at a) 34.3%TMD and b) 56.0%TMD.

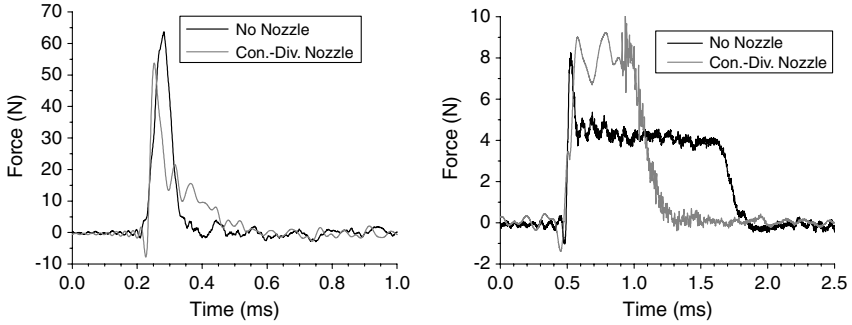

Fig. 8 Comparison of thrust with and without the nozzle in the a) fast regime and b) slow regime.

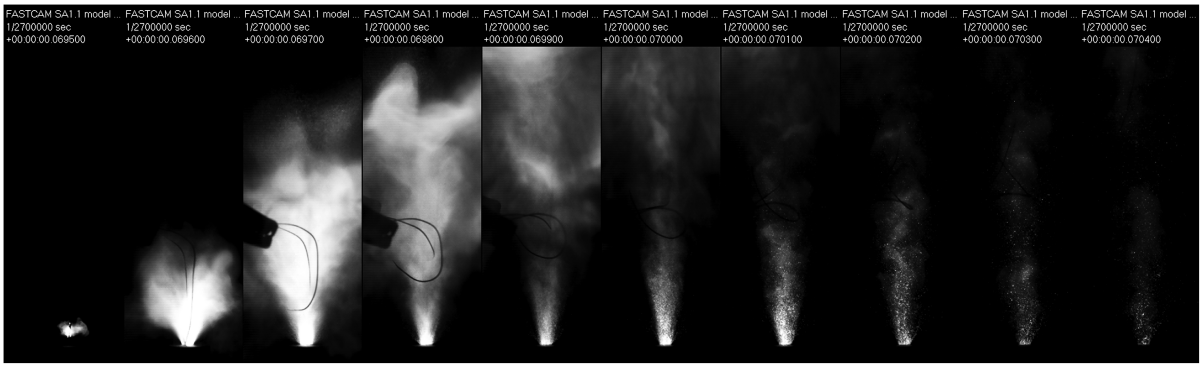

Fig. 9 Sequence of high-speed video frames from a thruster tested in the fast regime with the motor containing a convergent–divergent nozzle. There is 100 μs between each image (total time is 900 μs).

by the ejection of particulate material. However, based on the total time from start to finish of particle ejection, the convergent–divergent nozzle seems to prolong this process. The prolonging of the fluid ejection may be the reason for the reduction in peak thrust amplitude.

More insight into the reason that the nozzle slows the ejection of material in the fast-reaction regime may be gained by considering some of the conditions for ideal nozzle performance. One condition is that there is no friction or drag forces between the working fluid and the walls [13]. However, in the scale of the microthruster structure in this work, it is likely that friction between the working fluid and the thruster walls is not negligible.

Another condition for ideal rocket performance is that the working fluid does not contain any solid or liquid particles with significant size and/or mass [13]. It is evident from the images in Figs. 9 and 10, that there is a significant amount of solid/liquid particulates being ejected behind the main exhaust plume. It is possible that there are frictional forces between the particulates and the walls, and the convergent–divergent nozzle may enhance the effect of these forces.

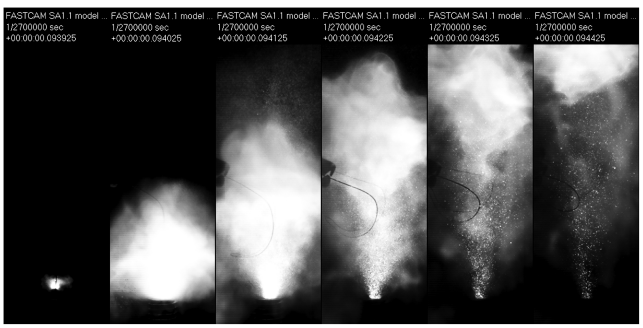

Fig. 10 Sequence of high-speed video frames from a thruster tested in the fast regime with the motor without a nozzle. There is 100 μs between each image (total time is 500 μs).

In other words, the net effect of the nozzle may be to decrease the mass flow rate and/or exit velocity of the reaction products. Consider the general formula for thrust force:

$$F = \dot{m}V_e + (p_e - p_0)A_e \tag{2}$$

where $\dot{m}$ is the mass flow rate, V_e is flow velocity at the nozzle exit plane, p_e is the pressure at the nozzle exit plane, p_0 is the ambient pressure, and A_e is the cross-sectional area at the nozzle exit plane. The nozzle may decrease the thrust force by reducing the first term of Eq. (2).

A further condition for ideal rocket performance is that the fluid flow is steady and continuous and the fluid expansion is uniform without shocks or discontinuities [13]. Again, this condition may not be met in the current system. It has been demonstrated that CuO/Al nanothermite composites can exhibit shock-wave-like behavior [8,14]. In particular, we have demonstrated previously that the formulation of CuO nanorods and Al nanoparticles are capable of producing shock waves when they are loaded at low packing densities, suggesting that such conditions will exist in the case of the fast-reaction regime of the current system; however, it is not fully understood how the presence of shock waves will change the function of the nozzle [8].

IV. Future Work

It appears that nanothermites have great potential for microthruster applications that require short-duration and high-amplitude thrust. We have plans to test various nanothermite formulations to understand the effect of gas production, reaction rate (including subsonic vs supersonic combustion), and reaction temperature on microthruster performance. Further work is also needed to understand the relationship between packing density and reaction-regime shift. It will improve motor efficiency if material can be loaded at higher density but still exhibit fast-reaction performance. Additionally, other system effects such as motor dimensions and structural material should be studied to determine the significance of energy

transfer with the chamber walls. It appears from this work that the nozzle may only cause increased friction between the fluid and the walls; however, different nozzle designs, such as simple converging or diverging nozzles, should also be tested to attempt to confirm this understanding. Eventually, a microelectromechanical system process will need to be developed that can incorporate the loading of the nanothermite fuel into the thruster and packaging of the device. In addition to improving the control over device geometry, it will also allow the effect of different ignition locations to be investigated. In the present system, ignition was triggered at the nozzle end of the thruster; however, there will likely be vastly different performance if the ignition is triggered at the end of the chamber opposite to the exit plane.

V. Conclusions

It has been demonstrated that CuO/Al nanothermites are capable of generating large-amplitude thrust compared with other fuels used in microthrusters. It has also been shown that the packing density of the composite can be chosen to control the regime of reaction (either fast or slow regimes) without significantly affecting the specific impulse that the material produces. Loading the material at relatively low %TMD causes the material to react in the fast regime, which results in short-duration high-amplitude thrust pulses. Additionally, in the fast-reaction regime, a convergent–divergent nozzle may not be necessary, due to significant deviations from ideal rocket performance conditions. This unique behavior of nanothermites in a microthruster is attributed to the unique characteristics of these nanopowder materials synthesized and self-assembled in the nanoscale.

Acknowledgments

We gratefully acknowledge the financial support by the U.S. Army Armament Research Development and Engineering Center and the fruitful discussions with Scott Kovaleski, University of Missouri.

References

[1] Ali, A., Son, S. F., Hiskey, M., and Naud, D., "Novel High Nitrogen Propellant Use in Solid Fuel Micropropulsion," *Journal of Propulsion and Power*, Vol. 20, No. 1, 2004, pp. 120–126. doi:10.2514/1.9238

[2] Lewis, D. H., Janson, S. W., Cohen, R. B., and Antonsson, E. K., "Digital Micropropulsion," *Sensors and Actuators A (Physical)*, Vol. 80, No. 2, 2000, pp. 143–154. doi:10.1016/S0924-4247(99)00260-5

[3] Chaalane, A., Rossi, C., and Este've, D., "The Formulation and Testing of New Solid Propellant Mixture (DB + x%BP) for a New Mems-Based Microthruster," *Sensors and Actuators A (Physical)*, Vol. 138, No. 1, 2007, pp. 161–166. doi:10.1016/j.sna.2007.04.029

[4] Zhang, K. L., Chou, S. K., and Ang, S. S., "Development of a Solid Propellant Microthruster with Chamber and Nozzle Etched on a Wafer Surface," *Journal of Micromechanics and Microengineering*, Vol. 14, No. 6, 2004, pp. 785–792. doi:10.1088/0960-1317/14/6/004

[5] Zhang, K. L., Chou, S. K., and Ang, S. S., "Development of a Low-Temperature Co-Fired Ceramic Solid Propellant Microthruster," *Journal of Micromechanics and Microengineering*, Vol. 15, No. 5, 2005, pp. 944–952. doi:10.1088/0960-1317/15/5/007

[6] Rossi, C., Larangot, B., Lagrange, D., and Chaalane, A., "Final Characterizations of MEMS-Based Pyrotechnical Microthrusters," *Sensors and Actuators A (Physical)*, Vol. 121, No. 2, 2005, pp. 508–514. doi:10.1016/j.sna.2005.03.017

[7] Groot, W. d., and Oleson, S., "Chemical Microthruster Options," NASA 1996, p. 19.

[8] Apperson, S., Shende, R., Subramanian, S., Tappmeyer, D., Gangopadhyay, S., Chen, Z., et al., "Generation of Fast Propagating Combustion and Shock Waves with Copper Oxide/Aluminum Nanothermite Composites," *Applied Physics Letters*, Vol. 91, No. 24, 2007, pp. 243109–3. doi:10.1063/1.2787972

[9] Shende, R., Subramanian, S., Hasan, S., Apperson, S., Thiruvengadathan, R., Gangopadhyay, K., et al., "Nanoenergetic Composites of CuO Nanorods, Nanowires, and Al-Nanoparticles," *Propellants, Explosives, Pyrotechnics*, Vol. 33, No. 2, 2008, pp. 122–130. doi:10.1002/prep.200800212

[10] Pantoya, M. L., and Granier, J. J., "Combustion Behavior of Highly Energetic Thermites: Nano versus Micron Composites," *Propellants, Explosives, Pyrotechnics*, Vol. 30, No. 1, 2005, pp. 53–62. doi:10.1002/prep.200400085

[11] Sanders, V. E., Asay, B. W.,Foley, T. J., Tappan, B. C., Pacheco, A. N., and Son, S. F., "Reaction Propagation of Four Nanoscale Energetic Composites (Al/MoO3, Al/WO3, Al/CuO, and Bi2O3)," *Journal of Propulsion and Power*, Vol. 23, No. 4, 2007, pp. 707–714. doi:10.2514/1.26089

[12] Prentice, D., Pantoya, M. L., and Gash, A. E., "Combustion Wave Speeds of Sol-Gel-Synthesized Tungsten Trioxide and Nano-Aluminum: The Effect of Impurities on Flame Propagation," *Energy and Fuels*, Vol. 20, No. 6, 2006, pp. 2370–2376. doi:10.1021/ef060210i

[13] Sutton, G. P., *Rocket Propulsion Elements*, 5th ed., Wiley, New York, 1986.

[14] Bulian, C. J., Smith, S., and Puszynski, J. A., "Experimental and Modeling Studies of Self-Sustaining Reactions Between Nanopowders," *2006 AIChe Annual Meeting* [CD-ROM], American Inst. of Chemical Engineers, New York, 2006.

S. Son
Associate Editor